Available online at www.sciencedirect.com
ScienceDirect
Chemical Physics Letters 438 (2007) 93–98
CHEMICAL PHYSICS LETTERS
www.elsevier.com/locate/cplett

Reaction force and electron localization function analysis of the metal chelation process in Mg(II)–thymine complex

Elizabeth Rincón, Alejandro Toro-Labbé *

Laboratorio de Química Teórica Computacional (QTC), Facultad de Química, Pontificia Universidad Católica de Chile, Casilla 306, Correo 22, Santiago, Chile

Received 25 October 2006; in final form 26 January 2007
Available online 9 February 2007

Abstract

The reaction force and the electron localization function (ELF) have been used to investigate the mechanism that promote the metal chelation in the formation of the Mg(II)–thymine *enol* bi-coordinated complex. Energy and reaction force profiles together with ELF isosurfaces reveal that the intramolecular hydrogen transfer activates the metal chelation process through a concentration of electron population in the monosynaptic valence basin associated to the hydrogen donor atom. Moreover, the ELF analysis suggest that the metal chelation proceeds via electrostatic interaction and the new Mg–N bond in the product complex being of ionic character.

1. Introduction

Metal migration processes generates metal-stabilized rare tautomers of nucleobases [1,2] which have been the subject of numerous studies mainly concerning their possible biological role in base-mispairing and mutagenesis [3]. This paper is concerned with the study of the Mg chelation process that occurs when going from the *keto* mono-coordinated Mg(II)–thymine complex to the *enol* bi-coordinated complex. The reaction is a two-steps process that involves a *keto* → *enol* tautomerization process followed by a reorientation of the O–Mg bond to allow a double coordination of magnesium with oxygen and nitrogen. Mg(II) is a hard cation with a low tendency to form covalent bonds [4]; in this context the characterization of the intramolecular chelation process and the nature of the Mg–thymine interaction is essential to understand its effects on the biological activity of metal–nucleobases complexes.

In order to get insights on the mechanism that promotes the metal chelation and the nature of the metal–nucleobase interaction, reaction regions defined from the reaction force profile are used as guidelines to the subsequent ELF analysis. In this paper we want to evaluate the performance of the electron localization function as a descriptor of the mechanism that leads to the formation of the Mg(II)–thymine complex in which the magnesium atom is simultaneously coordinated to an oxygen and a nitrogen atoms. On the other hand, the partition of the activation energy generated through the reaction force analysis is used to quantify the energy cost of the different processes that occur along the reaction coordinate.

2. Theory

2.1. The reaction force

The reaction force is the derivative of the potential energy ($E(\xi)$) with respect to the reaction coordinate ξ [5,6]:

$$F(\xi) = -\frac{dE}{d\xi} \tag{1}$$

For a generic potential function presenting an energy barrier separating the reactants, located at ξ_R, and the product at ξ_P, $F(\xi)$ exhibits two critical points (at points ξ_1 and ξ_2).

* Corresponding author. Fax: +56 2 686 4744.
E-mail address: atola@puc.cl (A. Toro-Labbé).

0009-2614/$ - see front matter © 2007 Elsevier B.V. All rights reserved.
doi:10.1016/j.cplett.2007.02.007

These are used to define three reaction regions along ξ: the reactant region ($\xi_R \leqslant \xi \leqslant \xi_1$) where the reactants gets prepared for the reaction mainly through structural reordering [7–11]; the transition state region ($\xi_1 < \xi < \xi_2$) which is characterized by a marked electronic reordering and the product region ($\xi_2 \leqslant \xi \leqslant \xi_P$) that is mainly characterized by structural relaxation leading to the products [7,9].

The work associated to a process occurring within a given interval along ξ is defined as

$$W_i = -\int_{\xi_i}^{\xi_i+\delta\xi_i} F(\xi)\mathrm{d}\xi \tag{2}$$

such that the activation energy can be defined as

$$\Delta E^{\neq} = \sum_{i=1}^{n} W_i \tag{3}$$

where n is the number of steps needed to reach the transition state. It is important to mention that Eq. (3) represents a rational way to partition the activation energy into contribution that might be associated to different physical processes thus throwing light on the nature of energy barriers. In the present case the partition of the energy barrier is dictated by the regions defined above, so that

$$\Delta E^{\neq} = W_1 + W_2 \tag{4}$$

with

$$W_1 = -\int_{\xi_R}^{\xi_1} F(\xi)\mathrm{d}\xi \quad \text{and} \quad W_2 = -\int_{\xi_1}^{\xi_0} F(\xi)\mathrm{d}\xi \tag{5}$$

where ξ_0 is the position of the transition state. Similarly the reaction energy is written as

$$\Delta E^{\circ} = W_1 + W_2 + W_3 + W_4 \tag{6}$$

where

$$W_3 = -\int_{\xi_0}^{\xi_2} F(\xi)\mathrm{d}\xi \quad \text{and} \quad W_4 = -\int_{\xi_2}^{\xi_P} F(\xi)\mathrm{d}\xi \tag{7}$$

In this way, $F(\xi)$ provides the elements to characterize reaction regions where different processes and mechanisms might be occurring, the energy associated to these processes is quantified through W_i ($i = 1,4$). In the present study the mechanisms that might be operating at the different regions will be identified through the analysis of the ELF function along the reaction coordinate.

2.2. The electron localization function

The ELF function $\eta(\mathbf{r})$ was first introduced by Becke and Edgecombe [12] as a descriptor of electronic localization, it is defined as

$$\eta(\mathbf{r}) = \frac{1}{1 + \left(\frac{D(\mathbf{r})}{D_h(\mathbf{r})}\right)^2} \tag{8}$$

where $D(\mathbf{r})$ is the excess of the local kinetic energy density due to the Pauli exclusion principle and $D_h(\mathbf{r})$ is the kinetic energy of an homogeneous electron gas with the same charge density $\rho(\mathbf{r})$, respectively [13–15]. The analytic form of Eq. (8) conveniently ranges $\eta(\mathbf{r})$ between 0 and 1; high values of $\eta(\mathbf{r})$ are associated to a high probability to find an electron pair [16]. The local maxima of $\eta(\mathbf{r})$ define the *core* and valence basins [14], the average population $\overline{N}_k$ associated to the kth basin is obtained from integration of the one-electron density $\rho(r)$ over the volume Ω_k:

$$\overline{N}_k(\Omega_k) = \int_{\Omega_k} \rho(\mathbf{r})\mathrm{d}\mathbf{r} \tag{9}$$

A measure of the quantum mechanical uncertainty of the population at the basin $\sigma^2(\overline{N}_k;\Omega_k)$ can also be defined:

$$\sigma^2(\overline{N}_k;\Omega_k) = \int_{\Omega_k} \mathrm{d}r_1 \int_{\Omega_k} \pi(\mathbf{r}_1,\mathbf{r}_2)\mathrm{d}r_2 + \overline{N}_k(\Omega_k) - [\overline{N}_k(\Omega_k)]^2 \tag{10}$$

where $\pi(\mathbf{r}_1,\mathbf{r}_2)$ is the probability of finding one electron at position $\mathbf{r}_1$ and another at $\mathbf{r}_2$ [17]. thus leading to the relative fluctuation of the population within the basin:

$$\lambda(\overline{N}_k) = \frac{\sigma^2(\overline{N}_k,\Omega_k)}{\overline{N}_k(\Omega_k)} \tag{11}$$

this quantity can be understood as a measure of the electron delocalization within the basin of volume Ω_k, usually a relative fluctuation larger than 0.45 is associated to delocalization [14].

Since the reaction depicted in Fig. 1 involves a proton transfer from N3 to O2 followed by the structural rearrangement of the O–Mg bond to allow the O–Mg–N3 double coordination, in the present work we will focus our attention on the analysis of the valence basins on N3, namely V1(N3) and V2(N3). The valence basins are characterized by the synaptic order, i.e. the number of core basins with which they have a common boundary or separatrix [18]. Monosynaptic basins, labeled V(X), correspond to electrons associated to a single atom X; disynaptic basins, labeled V(X,Y), are associated to bonds between atoms X and Y [19].

3. Methods and computational details

All calculations were carried out at the density functional theory (DFT) level, using the hybrid B3LYP functional [20,21] and the 6-311++G** basis set, using the GAUSSIAN 03 package [22]. Transition states were located using the quadratic synchronous transit (QST2) approach [23] and frequency calculations were performed in order to check the stationary states. The profiles of energy and reaction force were obtained through the intrinsic reaction coordinate (IRC) procedure [24]. This procedure defines the minimum energy path ξ connecting the transition state, whose position is arbitrarily assigned at $\xi_0 = 0$, with reactants and products at ξ_R and ξ_P, respectively. Infinitesimal displacements down from ξ_0 toward ξ_R and ξ_P define the numerical values of the reaction coordinate [25]. ELF cal-

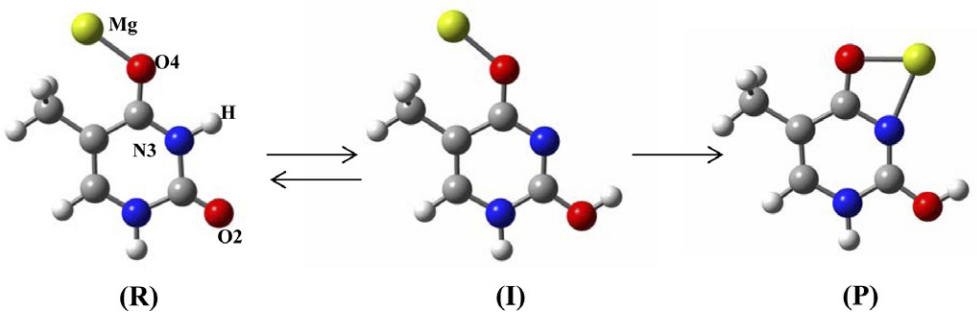

Fig. 1. Sketch of the reaction studied: the first step corresponds to the hydrogen transfer from N3 to O2; the second step corresponds to the metal migration toward N3.

culations were carried out at each point along the reaction coordinate ξ through the use of the TopMod program [25] and in order to assess the ELF results, they were compared to standard natural bond orbital populations (NBO) whose analysis was also performed [26].

4. Results and discussion

4.1. Energy and reaction force

Fig. 1 sketches the studied processes, the first step is the *keto* → *enol* tautomerization process in which the hydrogen is transferred from N3 to O2 to produce the *enol* intermediate Mg(II)–thymine mono-coordinated complex (**I**); the second step is the structural rearrangement of the O–Mg bond to allow a second coordination of Mg to N3 thus leading to the bi-coordinated Mg(II)–thymine complex. Fig. 2 display the energy and force profiles of the reaction, the first step $\mathbf{R} \rightarrow \mathbf{I}$ presents an energy barrier of $\Delta E_1^{\neq} = 44.21$ kcal/mol (Table 1) and a reaction energy practically equal to zero (0.45 kcal/mol) [27]. The second step $\mathbf{I} \rightarrow \mathbf{P}$ is characterized by a transition state (TS2) 0.64 kcal/mol above the *enol* mono-coordinated complex,

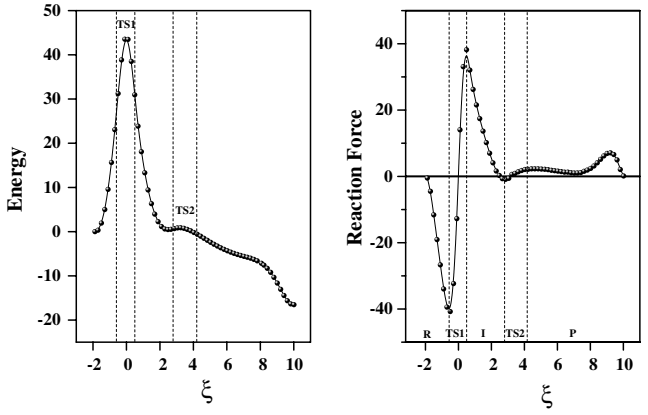

Fig. 2. Energy (in kcal/mol) and reaction force profiles (in kcal/mol·ξ) for the whole reaction depicted in Fig. 1. The dashed vertical lines indicate the limits of the reaction regions identified from the force profile: reactant (**R**); transition state 1 (TS1); intermediate (**I**); transition state 2 (TS2); product (**P**).

Table 1
Reaction energy (ΔE^0) and energy barriers for the hydrogen transfer ($\Delta E_1^{\neq}$) and for the metal migration ($\Delta E_2^{\neq}$)

ΔE^0	$\Delta E_1^{\neq}$	$\Delta E_2^{\neq}$	W_1	W_2	$-W_3$	$-W_4$
−19.11	44.21	0.64	27.11	17.10	9.37	53.95

Also displayed are the works associated to the different process that occur at the different reaction regions. All values in kcal/mol.

thus the bi-coordination process of Mg(II) can be considered as being spontaneous.

The critical points on the force profile defines reaction regions along ξ where the ELF analysis will be performed; these regions, shown in Fig. 2, are delimited by the dashed lines at $\xi_1 = -0.6$ and $\xi_2 = 0.5$ around the main transition state TS1 located at $\xi_0 = 0$; $\xi_3 = 2.8$ and $\xi_4 = 4.2$ surrounds the secondary transition state TS2 which is located at $\xi = 3.2$. In the first region the reaction is prepared mainly through structural reordering that helps promotes the hydrogen transfer. The second region is mainly characterized by electronic rearrangements that drives the hydrogen transfer and activates the reorientation of the O–Mg bond toward N3; the other three regions involve the bending of the O–Mg bond and the relaxation of the whole system to reach the product.

The amount work associated to the processes occurring within the reaction regions are $W_1 = -\int_{\xi_R}^{\xi_1} F(\xi)\mathrm{d}(\xi) = 27.11$ kcal/mol to activate the proton transfer; then the work $W_2 = -\int_{\xi_1}^{\xi_0} F(\xi)\mathrm{d}(\xi) = 17.10$ kcal/mol leads to the transition state (TS1) for the *keto* → *enol* tautomerization reaction. It is worth to notice that during the proton transfer, the metal cation remains at its original position until the geometry of the intermediate *enol* mono-coordinate complex, at about $\xi = 2.5$, is reached. In $W_3 = -\int_{\xi_0}^{\xi_2} F(\xi)\mathrm{d}(\xi) = -9.37$ kcal/mol are included the electronic reorder necessary to stabilize the newly formed O2–H bond and to activate the reorientation of the O4–Mg bond toward N3. An energy $W_4 = -\int_{\xi_2}^{\xi_P} F(\xi)\mathrm{d}(\xi) = -53.95$ kcal/mol, largely a structural relaxation energy, is then necessary to produce the *enol* bi-coordinated product from the *enol* mono-coordinated intermediate. It is interesting to note that $W_1 \approx -\frac{1}{2}W_4$ thus indicating that the reverse reaction is quite unfavorable due to a quite strong Mg–N bond

formed in the forward reaction. If only the electronic effects that are mainly present in W_2 and W_3 are considered, the reverse reaction appears to be favorable with an effective electronic activation energy which is about the half of that associated to the forward reaction ($W_3 \approx -\frac{1}{2}W_2$).

4.2. ELF analysis

In this section the monosynaptic basins bearing the non-bonded valence electrons attached to N3 are analyzed; Fig. 3 displays the profile of the average electronic population $\overline{N}$ on these monosynaptic basins and Table 2 quotes the associated values with their fluctuations.

In the reactant region there are two basins, V1(N3) and V2(N3), that present relative small populations ($\overline{N} = 0.61$e) which remain practically constant until ξ_1; the large relative fluctuations associated to populations of V1 and V2 indicates the participation of the N3 lone pair in the conjugate system ring at the first stage of the reaction. At the same time, an electronic population of about two electrons is localized on the disynaptic basin V(N3, H), as shown in Fig. 4, that displays the most relevant ELF basins at the reaction force key points along the reaction coordinate. It can be observed in Fig. 4 that as the proton is transferred to the oxygen atom (at the TS1 region) the disynaptic basin V(N3, H) splits while V1(N3) and V2(N3) coalesce to originate a unique basin V(N3), this new basin bears the electronic population coming from V1 and V2 plus the electrons coming out from the splitting of the V(N3, H) basin representing the N–H bond that is being broken. This explains the average total population of $\overline{N} \approx 3.0$e observed in Fig. 3 and quoted in Table 2. This population remains quite constant until reaching the product of the reaction whereas the relative fluctuations of the basin population displayed in Table 2 shows that from TS1 these electrons remain quite localized.

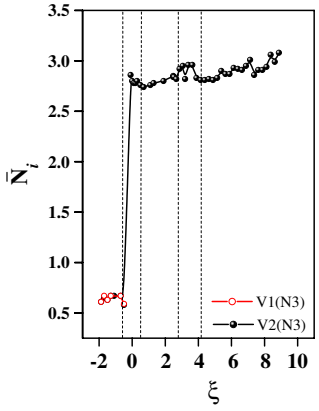

Fig. 3. Variation of the electronic populations ($\overline{N}$) associated to the lone pairs valence basins V1(N3) and V2(N3).

Table 2
Basins populations $\overline{N}$ on N3 and their relative fluctuations λ at the stationary points along the intrinsic reaction coordinate

Complex	V1/V		V2	
	$\overline{N}$	λ	$\overline{N}$	λ
Reactant	0.61	0.80	0.61	0.80
TS1	2.78	0.47	–	–
Intermediate	2.84	0.43	–	–
TS2	2.82	0.43	–	–
Product	3.08	0.43	–	–

Note that after the reactant region the V1 and V3 basins turn into the single basin V.

It is worth to mention that the electronic reordering that results in an increase of the population of the basin V(N3) at the TS1 region is associated with an energetic requirement $W_2 \approx 17$ kcal/mol (Table 1), energy that is used to populate the basin of N3 by breaking the aromatic delocalization observed in the reactant region and to prepare N3 for the metal chelation. In summary, it appears that the proton transfer activates the metal chelation process by localizing electrons on the basin V(N3), favoring in this way the electrostatic attraction with Mg(II), this being the driving force that produces the Mg–N3 bond.

Fig. 4 shows that in the reactant region the topological changes on the basins associated to the donor and acceptor atoms are quite small, this confirms that changes in this region are mainly of structural nature. In the TS1 region, the electronic rearrangements are observed with the formation of the short-lived basin V(H) while the hydrogen transfer is occurring; simultaneously the basin V(N3) (green)[1] starts to activate the reorientation of the O–Mg bond toward N3. Continuing the reaction in the other three regions, no significative changes are observed on V(N3) until the Mg–N3 bond is formed. This is evidence that structural reordering and relaxation are more important here than the electronic rearrangement, this is consistent with the large relaxation energy W_4 quoted in Table 1.

As already mentioned, NBO analysis [26] was performed to assess the information obtained through the electron localization function. Fig. 5 displays the total natural population on the N3 atom. It can be observed that in the reactant region, the electronic population increases slightly until the vicinity of ξ_1, then it decreases to reach a minimum value at about $\xi = 2.5$, at this point the hydrogen transfer is already completed. Then, in the product region the electronic population increases to reach a maximum at the bi-coordinated final product. In contrast to the ELF analysis, since the electronic population on N3 decreases when the intermediate (*enol*) mono-coordinate has been formed, the NBO analysis cannot explain the activating role played by the proton transfer localizing charge on N3 to produce the metal chelation; this is due to the fact that the natural charge reflects all the electronic reordering occurring on N3 whereas the more resolved electronic localization function allow to evaluate the electronic population $\overline{N}$ over the specific basins that are driving the reaction.

[1] For interpretation of color in Fig. 4, the reader is referred to the web version of this article.

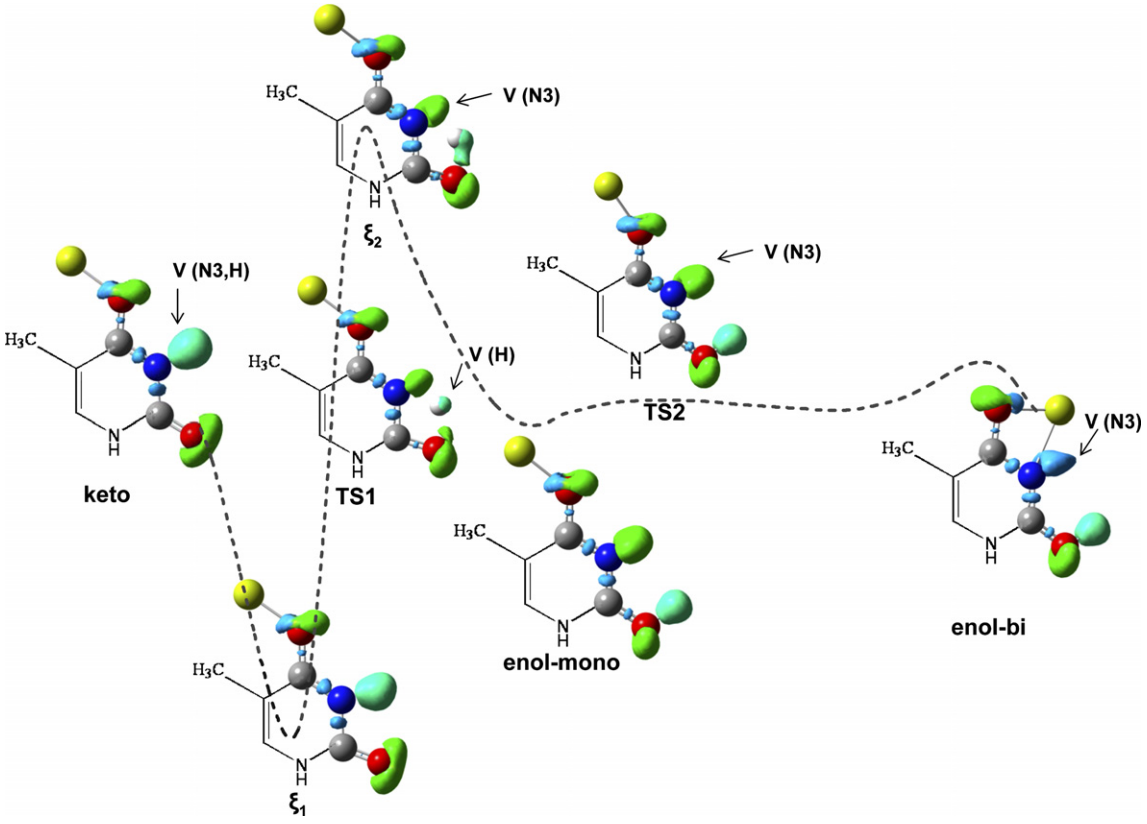

Fig. 4. ELF = 0.85 isosurfaces at the key points along the reaction force profile.

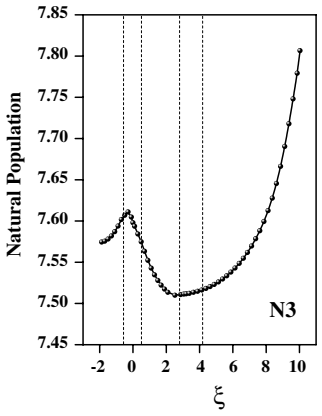

Fig. 5. Variation of the total natural population on N3 along the reaction coordinate.

Finally, it is worth to mention that the ionic nature of the Mg(II)–N3 bond in the product complex is established by the absence of a disynaptic valence basin of the type V(X, Y), a signature of a X–Y covalent bond [19,28,29]. This result was confirmed by the NBO analysis where a metal-to-ligand back donation was not observed.

5. Concluding remarks

The metal chelation process in the Mg(II)–thymine complex has been studied. The partition of the energy dictated by the reaction force profile together with the topological analysis of ELF in each region along the reaction coordinate has been useful to conclude that the hydrogen transfer promote the metal chelation process through the activation of the chelation site (N3) by localizing charge on it.

The energy necessary to activate the site has been partitioned into two contributions ($\Delta E_1^{\neq} = W_1 + W_2$), one associated to the structural preparation of the reactants ($W_1 = 27.1$ kcal/mol) and the other associated to electronic reordering that involves the proton transfer ($W_2 = 17.1$ kcal/mol). The electrostatic interaction Mg$\cdots$N3 thus produced being the driving force that leads to the ionic Mg–N3 bond at the product specie.

It can be concluded that the reaction force and ELF analysis provided an adequate description of the site activation mechanism for metal coordination and described correctly the ionic character of the Mg–N bond in the reaction product. The methodological features of reaction force and ELF presented in this work open the way to characterize chemical bonds and site activation mechanisms of more complex systems with potential technological applications such as catalizers or molecular electronic devices.

Acknowledgments

A.T.L. is indebted to the John Simon Guggenheim Foundation for a fellowship. This work has been supported by FONDECYT through Project No. 1060590

and FONDAP Project No. 11980002 (CIMAT). E.R. is grateful to DIPUC and MECESUP (PUC-0004, Red Química UCH-0116) for a graduate fellowship. The authors wish to thank Dr. Pablo Jaque (QTC@PUC) and Dr. Eduardo Chamorro (UNAB) for helpful discussions.

References

[1] B. Lippert, U. Schöllhorn, H. Thewalt, J. Am. Chem. Soc. 108 (1986) 6616.
[2] B. Lippert, Inorg. Chim. Acta 55 (1981) 5.
[3] M. Topal, J. Fresco, Nature 263 (1976) 285.
[4] M. Rodgers, J. Stanley, R. Amunugama, J. Am. Chem. Soc. 122 (2000) 10969.
[5] A. Toro-Labbé, J. Phys. Chem. A 103 (1999) 4398.
[6] J. Martínez, A. Toro-Labbé, Chem. Phys. Lett. 392 (2004) 132.
[7] S. Gutiérrez-Oliva, B. Herrera, A. Toro-Labbé, H. Chermette, J. Phys. Chem. A 109 (2005) 1748.
[8] P. Jaque, A. Toro-Labbé, J. Phys. Chem. A 104 (2000) 995.
[9] B. Herrera, A. Toro-Labbé, J. Chem. Phys. 121 (2004) 7096.
[10] A. Toro-Labbé, S. Gutiérrez-Oliva, M.C. Concha, J.S. Murray, P. Politzer, J. Chem. Phys. 121 (2004) 4570.
[11] P. Politzer et al., J. Chem. Sci. 117 (2005) 467.
[12] A. Becke, K. Edgecombe, J. Chem. Phys. 92 (1990) 5397.
[13] B. Silvi, A. Savin, Nature 371 (1994) 683.
[14] A. Savin, B. Silvi, F. Colonna, Can. J. Chem. 74 (1996) 1088.
[15] M. Kohout, A. Savin, Int. J. Quantum Chem. 60 (1996) 875.
[16] D. Marx, A. Savin, Angew. Chem., Int. Ed. Engl. 36 (1997) 2077.
[17] S. Noury, F. Colonna, A. Savin, B. Silvi, J. Mol. Struct. 450 (1998) 59.
[18] B. Silvi, J. Mol. Struct. 614 (2002) 3.
[19] J. Poater, M. Duran, M. Sola, B. Silvi, Chem. Rev. 105 (2005) 3911.
[20] A. Becke, J. Chem. Phys. 98 (1993) 5648.
[21] C. Lee, W. Yang, R. Parr, Phys. Rev. B 37 (1988) 785.
[22] M.J. Frisch et al., GAUSSIAN 03, Revision C.02, Gaussian Inc., Wallingford CT, 2004.
[23] C. Peng, P. Ayala, H. Schlegel, M. Frisch, J. Comput. Chem. 17 (1996) 49.
[24] K. Fukui, Acc. Chem. Res. 14 (1981) 363.
[25] S. Noury, X. Krodikis, F. Fuster, B. Silvi, Comput. Chem. 23 (1999) 597.
[26] A. Reed, L.A. Curtiss, F. Weinhold, Chem. Rev. 88 (1988) 899.
[27] E. Rincón, P. Jaque, A. Toro-Labbé, J. Phys. Chem. A 110 (2006) 9478.
[28] R.J. Gillespie, S. Noury, J. Pilme, B. Silvi, Inorg. Chem. 43 (2004) 3248.
[29] R.F.W. Bader, C.F. Matta, Int. J. Quantum Chem. 85 (2001) 592.